Geometry-induced Casimir suspension of oblate bodies in fluids

Alejandro W. Rodriguez,[1] M. T. Homer Reid,[2] Francesco Intravaia,[3,4] Alexander Woolf,[5] Diego A. R. Dalvit,[3] Federico Capasso,[5] and Steven G. Johnson[2]

[1]*Department of Electrical Engineering, Princeton University, Princeton, NJ 08540, USA*
[2]*Department of Mathematics, Massachusetts Institute of Technology, Cambridge, MA 02139, USA*
[3]*Theoretical Division, MS B213, Los Alamos National Laboratory, Los Alamos, NM 87545, USA*
[4]*School of Physics and Astronomy, The University of Nottingham, University Park, NG7 2RD Nottingham, United Kingdom*
[5]*School of Engineering and Applied Sciences, Harvard University, Cambridge, MA 02138, USA*

We predict that a low-permittivity oblate body (disk-shaped object) above a thin metal substrate (plate with a hole) immersed in a fluid of intermediate permittivity will experience a meta-stable equilibrium (restoring force) near the center of the hole. Stability is the result of a geometry-induced transition in the sign of the force, from repulsive to attractive, that occurs as the disk approaches the hole—in planar or nearly-planar geometries, the same material combination yields a repulsive force at all separations in accordance with the Dzyaloshinskiĭ–Lifshitz–Pitaevskiĭ condition of fluid-induced repulsion between planar bodies [1]. We explore the stability of the system with respect to rotations and lateral translations of the disks, and demonstrate interesting transitions (bifurcations) in the rotational stability of the disks as a function of their size. Finally, we consider the reciprocal situation in which the disk–plate materials are interchanged, and find that in this case the system also exhibits meta-stability. The forces in the system are sufficiently large to be observed in experiments and should enable measurements based on the diffusion dynamics of the suspended bodies.

PACS numbers:

Casimir forces arising from quantum/thermal fluctuations of charges are becoming increasingly important in nano- and micro-scale systems [2–9], where the usually attractive nature of the force leads to unwanted effects such as stiction [8]. Recent theoretical developments have made it possible to study the influence of geometry and materials on these interactions [8, 10]; for instance, geometry effects alone can lead to unusual behaviors, including non-monotonic and/or repulsive forces between vacuum-separated bodies [11–13]. For planar geometries, one way to obtain repulsion is to employ fluids [1, 14, 15]. Dzyaloshinskiĭ *et. al.* showed decades ago that two planar bodies of permittivities $\varepsilon_{1,2}$ immersed in a fluid of permittivity ε_3, satisfying $\varepsilon_1 < \varepsilon_3 < \varepsilon_2$ will repel one another [1], an effect that has also been observed in experiments [16, 17]. Based on that prediction, one might ask whether the Dzyaloshinskiĭ–Lifshitz–Pitaevskiĭ (DLP) condition alone suffices to obtain repulsion regardless of geometry. In this letter, we exploit a recently developed numerical method for computing Casimir interactions between arbitrary bodies [18] to answer this question in the negative. Specifically, we show that the Casimir potential between an oblate body (a disk-shaped object) and a thin metal substrate (a plate with a hole) immersed in a fluid satisfying the DLP condition exhibits a meta-stable equilibrium at the center of the hole, creating a "Casimir trap" for the disk.

Although Casimir suspensions are impossible for vacuum-separated bodies (irrespective of geometry) [19, 20], they can arise in fluids satisfying the DLP condition [21–23]. The approach described here differs from previous work in that it does not rely on material dispersion [23] or the presence of external forces (e.g. gravity [22]), nor does it require bodies to be enclosed inside one another [21, 24], but instead stems from the anomalous behavior of electromagnetic fields in this particular geometry (shown schematically in Fig. 1). In recent work [13], we exploited a similar geometric effect to demonstrate the possibility of switching the sign of the Casimir force between two *vacuum*-separated bodies—a small, metallic, *prolate body* (thin needle) centered above a metal plate with a hole—from attractive to *repulsive*. That phenomenon was explained via a simple symmetry argument [13]: because the fields of a needle in vacuum behave like those of a dipole oriented along its symmetry axis, its interaction with a plate decreases as the needle reaches the center of the hole (at which point the field lines become orthogonal to the plate). The same symmetry argument (in conjunction with a more sophisticated dipole model) is employed here to show that in water, the interaction between a small Polutetraflouroethylene (PTFE) body and a thin gold (Au) plate with a hole can be switched from repulsive to *attractive* near the vicinity of the hole. To our surprise, however, the interesting geometry in this case is not a needle but rather an *oblate body* (thin disk), a consequence of the flipped polarization-response of the disk in the fluid. We quantify deviations from dipole-like behavior by comparing our Casimir predictions against a corresponding Casimir–Polder (CP) model in which the disk is modelled as a dipole of equivalent polarizability, and show that finite-size effects can lead to significant qualitative and quantitative deviations for large disks and small separations. Interestingly, despite these deviations, we find that the desired geometric effects persist even for *large* disks (with diameters $\sim$ hole size), leading to much larger forces than those predicted in the vacuum case. Moreover, unlike the vacuum case (in which the needle must be anchored to a static surface [13, 25]), here the disks are stable with respect to rotations and/or lateral translations, and are therefore free to move subject to Brownian motion. This enables exploration of this phenomenon through

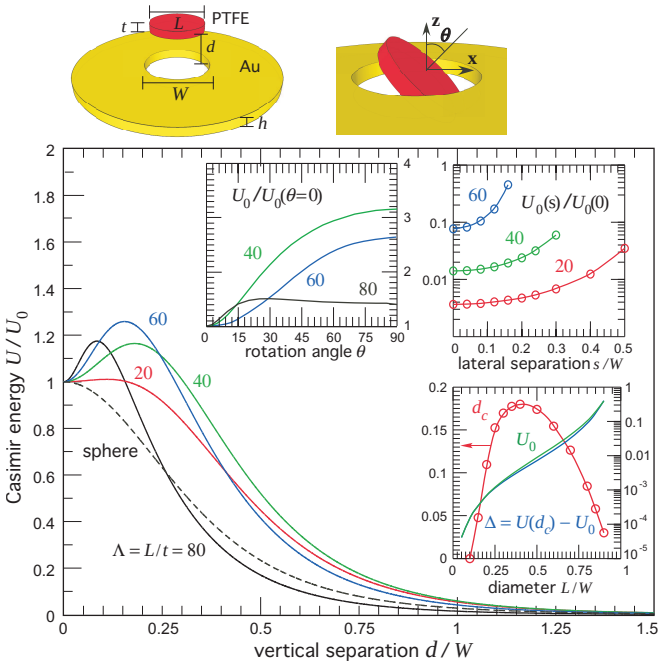

FIG. 1: Room-temperature Casimir energy U of a PTFE disk (thickness $t = 10$nm) suspended above a Au plate (thickness $h = 10$nm and inner and outer diameters $W = 1\mu$m and $D = 2W$) immersed in water, as a function of vertical separation d (normalized by W). U is normalized by the energy in the co-planar configuration, $U_0 \equiv U(d = 0)$, and plotted for multiple aspect ratios $\Lambda = L/t$, where L is the disk diameter. Also shown is the energy of a sphere of diameter $20t$ (dashed black line). (Top insets:) U as a function of rotation angle θ (left) and lateral translations s (right) for multiple Λ. (Bottom inset:) unstable equilibrium separation d_c (red circles), along with the energy U_0 (green line) and corresponding energy barrier $\Delta = U(d_c) - U_0$ (blue line), normalized by $k_BT \approx 25$meV, as a function of L. Both d_c and L are normalized by W.

a broader set of experimental techniques, e.g. measurements based on total-internal reflection microscopy or diffusion dynamics. Finally, we consider the "reciprocal" situation involving a Au disk above a PTFE plate, and find that in that case one also obtains a meta-stable equilibrium, albeit with larger geometric anisotropy leading to larger energy barriers.

Figure 1 shows the room-temperature Casimir energy U between a PTFE disk and a co-axial Au plate immersed in water, as a function of their mutual center–center separation d. U is normalized by the energy U_0 when the two bodies are coplanar ($d = 0$) and is plotted for multiple aspect ratios $\Lambda = L/t$ (keeping t fixed). The Au dielectric permittivity is obtained from a Drude model with plasma frequency $\omega_p = 9$eV and damping constant $\gamma = 0.035$eV, whereas the PTFE and water permittivities are obtained using the oscillator models described in Ref. 26. This specific material combination was chosen because it satisfies the DLP condition of fluid repulsion between planar bodies—indeed, we find that the force between a finite disk and an unpatterned ($W = 0$) plate is repulsive over all d and diverges as $d \to 0$ (not shown). As expected, and in contrast to the unpatterned case, the presence of the hole means that U no longer diverges as $d \to 0$ but instead reaches a finite constant (so long as $L < W$). We find that for spheres (dashed black line), nearly-isotropic, or prolate bodies, U increases monotonically with decreasing d, attaining its peak at $d = 0$ as expected. The situation is different for oblate bodies ($\Lambda > 1$), in which case U peaks at a critical separation $d_c > 0$ (determined by Λ), below which the force transitions from repulsive to *attractive*. In particular, instead of the usual unstable equilibrium, we find that the disk exhibits a *meta-stable* equilibrium at $d = 0$. In order to investigate the full stability of the disk, and its dependence on Λ, the top insets in Fig. 1 show the energy of the system in the co-planar configuration ($d = 0$) as a function of rotation θ and lateral translations s of the disk, for multiple Λ. Our results reveal that whenever Λ is either too small or too large, the non-monotonicity in the potential (and corresponding meta-stability) disappears. Specifically, we find that d_c and the corresponding potential barrier $\Delta = U(d_c) - U_0$ vanish as $L \to 0$ and $L \to W$ (not shown in the figure), respectively. Moreover, while the disk is repelled from the edges of the hole irrespective of Λ, its stability with respect to rotations changes drastically with increasing L/W. In particular, beyond $L \approx 0.7W$, corresponding to $\Lambda \approx 80$, additional unstable and stable equilibria appear at (a finite) $\theta_c > 0$ and $\theta = 90°$, respectively. For $L \gtrsim 0.9W$ (not shown), corresponding to $\Lambda \approx 90$, the preferred orientation of the disk (the minimum U) changes from $\theta = 0$ (parallel) to $\theta = 90°$ (perpendicular). In the perpendicular orientation, the potential barrier $\Delta \to 0$ and the disk is repelled from the hole.

In order to understand the above features as well as the origin of the non-monotonicity in U, it is useful to examine the Casimir-energy imaginary-frequency spectrum $U(i\xi)$ of the system , whose integral (a Matsubara sum at finite temperatures [8]) yields U. The bottom inset of Fig. 2 shows $U(i\xi)$ for a representative disk–plate configuration exhibiting non-monotonicity ($\Lambda = 60$) at multiple separations $d = \{0, 0.2, 0.4\}W$, and illustrates that non-monotonicity in d is present only at small "quasistatic" ξ. In this quasistatic regime, a thin disk immersed in a fluid of larger permittivity will act like a fluctuating dipole oriented mainly along its symmetry axis [33]. In contrast, the same disk in vacuum will be mainly polarized in the direction *transverse* its axis of symmetry (as shown below). Since the fields generated by a fluctuating dipole lie mainly along the dipole axis and become orthogonal to the metal plate as $d \to 0$, it follows that the disk–plate interaction will weaken in the vicinity of the hole [13], leading to the behavior above.

In what follows, we quantify the previous argument via a simple model in which the disk is described as a dipole with an effective polarizability, corresponding to the leading-order term of a spherical-harmonic expansion in the scattering formalism [28]. The zero-temperature CP energy between a polarizable particle at position $\mathbf{x}$ and the plate can be written

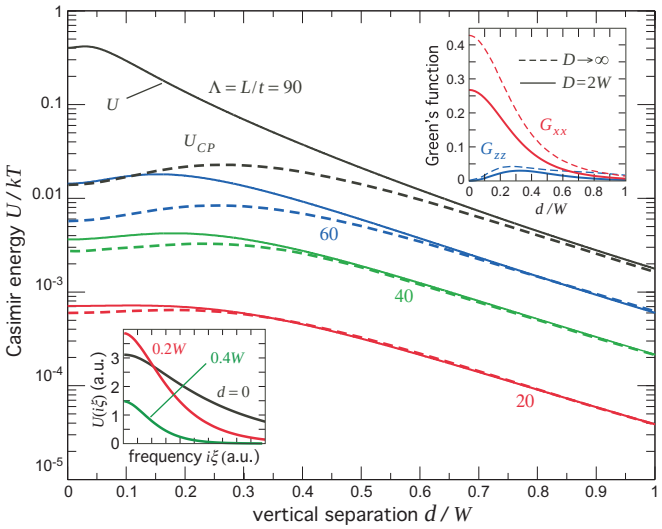

FIG. 2: Room-temperature Casimir U (solid lines) and Casimir–Polder U_{CP} (dashed lines) energies, normalized by $k_BT \approx 25meV$, for the disk–plate geometry of Fig. 1, as a function of d (normalized by W), plotted for multiple aspect-ratios $\Lambda = L/t$. U_{CP} is obtained from the polarizability of the disks, as determined by Eq. 2. (Top inset:) diagonal components of the photon GF of the plate evaluated along the axis of symmetry, for both finite $D = 2W$ (solid lines, evaluated numerically) and semi-infinite $D \to \infty$ PEC (dashed lines, evaluated anaytically [27]) plates. (Bottom inset:) Casimir integrand $U(i\xi)$, in arbitrary units, as a function of imaginary frequency $i\xi$ at three different separations $d = \{0, 0.2, 0.4\}W$, for $\Lambda = 60$.

as [9, 29]:

$$U_{CP} = -\frac{\hbar}{2\pi}\int_0^\infty d\xi\ \mathrm{Tr}\left[\boldsymbol{\alpha}(i\xi)\cdot\mathbb{G}(i\xi;\mathbf{x},\mathbf{x})\right], \qquad (1)$$

where $\boldsymbol{\alpha}(i\xi)$ and $\mathbb{G}(i\xi,\mathbf{x},\mathbf{x})$ are the imaginary-frequency dipole polarizability and Dyadic Green's function (GF) of the plate in the surrounding medium evaluated at the location of the dipole.

Although the polarizability of a disk of permittivity ε_1, diameter L, height t, and corresponding volume $V = \pi L^2 t$, surrounded by a medium of permittivity ε_3, cannot be easily computed analytically, it is nevertheless well approximated by that of a spheroidal body of similar dimensions [30, 31]. In that case, the polarizability in the jth direction,

$$\alpha_j = \varepsilon_3^2 V \frac{\tau - 1}{1 + (\tau - 1)n_j}, \qquad (2)$$

is determined by the ratio $\tau \equiv \varepsilon_1/\varepsilon_3$ and depolarization factors, $n_{x,y} = \frac{1}{2}(1 - n_z)$ and

$$n_z = \begin{cases} \frac{1-e^2}{2e^3}\left[\log\left(\frac{1+e}{1-e}\right) - 2e\right], & t < L \\ \frac{1+e^2}{e^3}\left[e - \arctan(e)\right], & t > L, \end{cases} \qquad (3)$$

where $e = \sqrt{|1 - (t/L)^2|}$ is the eccentricity of the body [31].

To qualitatively explain the behavior observed in Fig. 1, it suffices to restrict our analysis to the asymptotic limits of either an elongated "needle" (a prolate body with $t \gg L$) or a flat "disk" (an oblate body with $t \ll L$), in which case

$$\alpha_z = \varepsilon_3^2 V \begin{cases} \tau - 1, & t \gg L \\ 1 - \frac{1}{\tau}, & t \ll L \end{cases}, \quad \alpha_{x,y} = \varepsilon_3^2 V \begin{cases} 2\frac{\tau-1}{\tau+1}, & t \gg L \\ \tau - 1, & t \ll L \end{cases}. \qquad (4)$$

Matters simplify further in the limit of large index contrast ($\tau \ll 1$ or $\tau \gg 1$), in which case the CP energies of the needle U_{needle} and disk U_{disk} take the form:

$$U_{needle} = -\varepsilon_3^2 V \begin{cases} \tau G_{zz}, & \tau \gg 1 \\ -G_{zz} - 2(G_{xx} + G_{yy}), & \tau \ll 1 \end{cases} \qquad (5)$$

$$U_{disk} = -\varepsilon_3^2 V \begin{cases} \tau(G_{xx} + G_{yy}), & \tau \gg 1 \\ -\frac{1}{\tau}G_{zz}, & \tau \ll 1, \end{cases} \qquad (6)$$

where $G_{kk} \equiv G_{kk}(i\xi;\mathbf{x},\mathbf{x})$. In the case of an infinitesimally thin perfect electric conductor (PEC) plate (corresponding to $\varepsilon_2 \to \infty$, $h \to 0$, and $D \to \infty$ in our geometry) with a hole of size W, one can write down an analytical expression for $G_{kk}(0;\mathbf{x},\mathbf{x})$ in the non-retarded limit [27, 32]. For a dipole centered along the axis of symmetry of the plate, i.e. $\mathbf{x} = \{0, 0, d\}$, one finds that G_{zz} exhibits local minima and maxima at $d = 0$ and $d = d_c \approx W/3$, respectively, while $G_{xx} = G_{yy} (\gg G_{zz})$ decreases monotonically with separation [27]. Both GF components are plotted versus d on the top inset of Fig. 2 (dashed lines). It follows from Eq. 5 that a needle will experience a repulsive (attractive) force for $d < d_c$ ($d > d_c$) in the $\tau \gg 1$ regime, as was predicted in Ref. 13, and a repulsive force at all separations in the $\tau \ll 1$ regime, in agreement with predictions based on the DLP condition. In contrast, however, Eq. 6 predicts that a disk will experience an attractive force at all separations in the $\tau \gg 1$ regime, and an attractive (repulsive) force for $d < d_c$ ($d > d_c$) in the $\tau \ll 1$ regime, in qualitative agreement with our results above.

In order to incorporate effects coming from the finite size/thickness of the plate, as well as to quantify deviations from the dipole picture that arise in the $L \to W$ and $d \to 0$ limits, we compare our results of Fig. 1 to the corresponding CP potential of the system, obtained via Eq. 1 by assuming a spheroidal particle with polarizability given by Eq. 2 and with $\mathbb{G}(i\xi)$ computed numerically. As expected, the GFs of the finite Au plate, plotted in the $\xi \to 0$ limit on the top inset of Fig. 2 (solid lines), are smaller than those of the semi-infinite PEC plate (due to its smaller surface area), but exhibit the same anomalous behavior. (Away from the quasistatic regime, corresponding to larger ξ, G_{zz} exhibits non-monotonicity but τ tends to unity, causing the object to appear more isotropic as can be seen from Eq. 2, and leading to the dissapearance of this effect.) Figure 2 shows both U_{CP} and the Casimir energy U versus d, for multiple values of Λ (with t fixed as before), showing agreement at large d and small Λ, a regime where the disks behave like ideal (isolated) dipoles. In the opposite limit of large $\Lambda \gg 1$ (corresponding to $L \sim W$), the outer and inner surfaces of the disk and plate approach one another (touching as $d \to 0$ for $L \geq W$), thereby causing the interaction energy to be dominated by proximity effects [9]. This transition

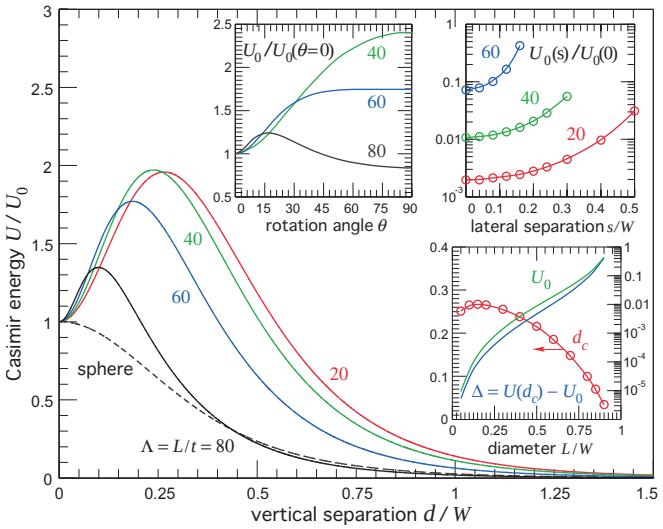

FIG. 3: Room-temperature Casimir energy U as a function of d for the disk–plate geometry of Fig. 1, but with the Au and PTFE materials interchanged. U is normalized by U_0 and plotted for multiple values of Λ. (Top insets:) U as a function of rotation angle θ (left) and lateral translations s (right) for multiple Λ. (Bottom inset:) unstable equilibrium separation d_c (red circles), along with U_0 (green line) and $\Delta = U(d_c) - U_0$ (blue line), normalized by $k_BT \approx 25\text{me}V$, as a function of L. Both d_c and L are normalized by W.

manifests itself in multiple ways: First, though the CP model predicts a monotonically increasing d_c with increasing L, we find instead that in the finite system, d_c reaches a maximum at $L \approx 0.4W$ and then *decreases* as $L \to W$ (red circles on the bottom inset of Fig. 1). Second, while the dipole picture predicts a monotonically increasing $U_{CP} \sim L^2$ (stemming from the linear dependence of the polarizability with the disk volume), the dependence of U_0 on L exhibits a power-law *divergence* that scales as $1/(W-L)^\beta$, with $\beta \approx 5/2$, in the limit as $L \to W$ (green line on the bottom inset of Fig. 1). The same proximity effects are responsible for a dramatic increase in Δ (blue line) with increasing L. We note however, that the competition between increasing U and decreasing nonmonotonicity eventually skews in favor of the latter causing a peak in Δ as $L \to W$ and eventually causing $\Delta \to 0$ in this limit (not shown in the figure).

Figure 3 shows the ratio U/U_0 for the same geometry of Fig. 1 but for the "reciprocal" situation where the Au and PTFE materials are interchanged (corresponding to a Au disk above a PTFE plate). As before, the insets explore the stability of the system with respect to rotations and lateral translations of the disk. In this case, the polarizability of the disk is largest along the lateral (x–y) directions, and hence the relevant equation describing the resulting CP interaction is the top equation of Eq. 6. However, unlike the previous case, here it is the G_{xx} and G_{yy} components of the DGF (and not G_{zz}) that exhibit non-monotonicity, leading again to a meta-stable equilibrium at $d = 0$, albeit with slightly smaller U and significantly larger non-monotonicity for the same Λ. Essentially, the index contrast between the Au disk and the fluid is orders of magnitude larger than for a PTFE disk, leading to larger polarization anisotropies. Unfortunately, the enhanced anisotropy comes at a price: First, the small index contrast between the plate and the fluid results in a smaller U, a consequence of the larger contribution of the plate area. Second, the transition in the preferred orientation of the disk from $\theta = 0 \to 90^\circ$ occurs at smaller Λ. The large polarization anisotropy of the Au disk also means that the potential trap is not very sensitive to the disk thickness. Fixing $h = 10\text{nm}$ and $L = 0.6W$, we find that $\Delta \to 2\Delta$ and $U_0 \to 5U_0$ as t is increased from $t = 10\text{nm} \to 100\text{nm}$ (corresponding to a decrease in Λ from $\Lambda = 60 \to 6$). On the other hand, we find that Δ is very sensitive to changes in the PTFE plate thickness. Fixing $t = 10\text{nm}$ and $L = 0.6W$, we find that $\Delta \to 0$ rapidly as h is increased from $h = 10\text{nm} \to 100\text{nm}$. The situation is reversed in the reciprocal configuration of Fig. 1, in which case the trap is sensitive to the disk thickness and not the plate thickness.

The system described in this work constitutes a promising platform to investigate two unusual geometry-induced Casimir phenomena: a violation of the DLP condition of fluid repulsion between planar bodies, and the stable suspension of two bodies. At room temperature, the resulting "Casimir trap" has a depth on the order of k_BT, which, unlike the case of a needle in vacuum [13], allows for simpler (and more varied) experimental verification of this phenomenon. It could also open new horizons for technological applications where passive suspension is relevant. We believe that even more pronounced effects should arise in other geometries and material configurations. For instance, stronger potential traps might be obtained by designing the shapes of the suspended bodies to exhibit larger polarization anisotropy, a subject of future work.

This work was supported by DARPA Contract No. N66001-09-1-2070-DOD, by the AFOSR Multidisciplinary Research Program of the University Research Initiative (MURI) for Complex and Robust On-chip Nanophotonics, Grant No. FA9550-09-1-0704, and by the U.S. Army Research Office under contracts W911NF-07-D-0004 and W911NF-13-D-0001.

[1] I. E. Dzyaloshinskiĭ, E. M. Lifshitz, and L. P. Pitaevskiĭ, Adv. Phys. **10**, 165 (1961).
[2] H. B. G. Casimir, Proc. K. Ned. Akad. Wet. **51**, 793 (1948).
[3] K. A. Milton, J. Phys. A **37**, R209 (2004).
[4] S. K. Lamoreaux, Phys. Today **60**, 40 (2007).
[5] C. Genet, A. Lambrecht, and S. Reynaud, Eur. Phys. J. Special Topics **160**, 183 (2008).
[6] M. Bordag, G. L. Klimchitskaya, U. Mohideen, and V. M. Mostapanenko, *Advances in the Casimir Effect* (Oxford University Press, Oxford, UK, 2009).
[7] G. L. Klimchitskaya, U. Mohideen, and V. M. Mostapanenko, Rev. Mod. Phys. **81**, 1827 (2009).
[8] A. W. Rodriguez, F. Capasso, and S. G. Johnson, Nat. Phot. **5**, 211 (2011).
[9] D. A. R. Dalvit, P. Milonni, D. Roberts, and F. da Rosa, eds.,

Lecture Notes in Physics, vol. 834 (Springer-Verlag, 2011).
[10] S. G. Johnson, in *Casimir Physics*, edited by D. A. R. Dalvit, P. Milonni, D. Roberts, and F. d. Rosa (Springer–Verlag, 2011), vol. 836 of *Lecture Notes in Physics*, chap. 6, pp. 175–218.
[11] A. Rodriguez, M. Ibanescu, D. Iannuzzi, F. Capasso, J. D. Joannopoulos, and S. G. Johnson, Phys. Rev. Lett. **99**, 080401 (2007).
[12] P. Rodriguez-Lopez, S. J. Rahi, and T. Emig, Phys. Rev. A **80**, 022519 (2009).
[13] M. Levin, A. P. McCauley, A. W. Rodriguez, M. T. H. Reid, and S. G. Johnson, Phys. Rev. Lett. **105**, 090403 (2010).
[14] J. N. Israelachvili, *Intermolecular and Surface Forces* (Academic Press, London, 1991).
[15] A. V. Parsegian, *Van der Waals Forces: A Handbook for Biologists, Chemists, Engineers, and Physicists* (Cambridge University Press, NY, 2006).
[16] A. A. Feiler, L. Bergstrom, and M. W. Rutland, Langmuir **24**, 2274 (2008).
[17] J. Munday, F. Capasso, and V. A. Parsegian, Nature **457**, 170 (2009).
[18] H. Reid, J. White, and S. G. Johnson, Phys. Rev. A. Rapid. Comm. **84**, 010503 (2011).
[19] O. Kenneth and I. Klich, Phys. Rev. Lett. **97**, 160401 (2006).
[20] S. J. Rahi, M. Kardar, and T. Emig, Phys. Rev. Lett. **105**, 070404 (2010).
[21] A. W. Rodriguez, J. Munday, D. Davlit, F. Capasso, J. D. Joannopoulos, and S. G. Johnson, Phys. Rev. Lett. **101**, 190404 (2008).
[22] A. P. McCauley, A. W. Rodriguez, J. D. Joannopoulos, and S. G. Johnson, Phys. Rev. A **81**, 012119 (2010).
[23] A. W. Rodriguez, A. P. McCauley, D. Woolf, F. Capasso, J. D. Joannopoulos, and S. G. Johnson, Phys. Rev. Lett. **104**, 160402 (2010).
[24] S. J. Rahi and S. Zaheer, Phys. Rev. Lett. **104**, 070405 (2010).
[25] A. P. McCauley, A. W. Rodriguez, M. T. H. Reid, and S. e. G. Johnson, arXiv **1105.0404** (2011).
[26] P. J. van Zwol and G. Palasantzas, Phys. Rev. A **81**, 062502 (2010).
[27] C. Eberlein and R. Zietal, Phys. Rev. A **83**, 052514 (2011).
[28] T. Emig, N. Graham, L. R. Jaffe, and M. Kardar, Phys. Rev. A **79**, 054901 (2009).
[29] H. B. G. Casimir and D. Polder, Phys. Rev. **13**, 360 (1948).
[30] H. C. van de Hulst, *Light scattering by small particles* (Dover Publications, 1957).
[31] J. Venermo and A. Sihvola, J. Electrostatics **63**, 101 (2005).
[32] K. A. Milton, E. K. Abalo, P. Parashar, and N. Pourtolami, Phys. Rev. A **83**, 062507 (2011).
[33] Strictly speaking, the dipole limit requires $L \ll W \ll d$.